



This is a repository copy of *Statistical EOF analysis of spatiotemporal glacier mass-balance variability: a case study of Mittivakkat Gletscher, SE Greenland*.

White Rose Research Online URL for this paper:

<https://eprints.whiterose.ac.uk/122869/>

Version: Accepted Version

Article:

Mernild, S.H., Beckerman, A.P. orcid.org/0000-0002-4797-9143, Knudsen, N.T. et al. (2 more authors) (2018) Statistical EOF analysis of spatiotemporal glacier mass-balance variability: a case study of Mittivakkat Gletscher, SE Greenland. *Geografisk Tidsskrift-Danish Journal of Geography*, 118 (1). pp. 1-16. ISSN 0016-7223

<https://doi.org/10.1080/00167223.2017.1386581>

Reuse

Items deposited in White Rose Research Online are protected by copyright, with all rights reserved unless indicated otherwise. They may be downloaded and/or printed for private study, or other acts as permitted by national copyright laws. The publisher or other rights holders may allow further reproduction and re-use of the full text version. This is indicated by the licence information on the White Rose Research Online record for the item.

Takedown

If you consider content in White Rose Research Online to be in breach of UK law, please notify us by emailing eprints@whiterose.ac.uk including the URL of the record and the reason for the withdrawal request.



eprints@whiterose.ac.uk
<https://eprints.whiterose.ac.uk/>

1 **Statistical EOF analysis of spatiotemporal glacier**
2 **mass-balance variability: A case study of**
3 **Mittivakkat Gletscher, SE Greenland**

4
5 SEBASTIAN H. MERNILD

6 *Nansen Environmental and Remote Sensing Center, Bergen, NORWAY*
7 *Faculty of Engineering and Science, Western Norway University of Applied Science, Sogndal,*
8 *NORWAY*
9 *Antarctic and Sub-Antarctic Program, Universidad de Magallanes, Punta Arenas, CHILE*

10
11 ANDREW P. BECKERMAN

12 *Department of Animal and Plant Sciences, University of Sheffield, UK*

13
14 NIELS TVIS KNUDSEN

15 *Department of Geoscience, Aarhus University, Aarhus, DENMARK*

16
17 BENT HASHOLT

18 *Department of Geosciences and Natural Resource Management, University of Copenhagen,*
19 *DENMARK*

20
21 JACOB C. YDE

22 *Faculty of Engineering and Science, Western Norway University of Applied Science, Sogndal,*
23 *NORWAY*

24
25 *Accepted Danish Journal of Geography, September 27, 2017*

26
27 Corresponding author address:

28 Dr. Scient. Sebastian H. Mernild

29 E-mail: sebastian.mernild@nersc.no

30 **Abstract**

31 An Empirical Orthogonal Function (EOF) variance analysis was performed to map and elucidate
32 in detail the spatiotemporal variability in individual stake mass-balances (b_a) on the Mittivakkat
33 Gletscher (MG) – in a region where at present five out of ~20.000 glaciers have mass-balance
34 observations. The EOF analysis suggested that observed b_a was summarized by two major
35 modes: EOF1 and EOF2 represented 80 % (significant) and 6 % (insignificant) of the explained
36 variance, respectively. EOF1 captured a decline in b_a that was uniformly distributed in space at
37 all stakes. The decline was correlated with: 1) albedo observations; and 2) surface air
38 temperature observations from nearby maritime and coastal stations. EOF2, however, described
39 variations in b_a that were heterogeneously distributed among stakes and associated with local
40 slope and aspect. Low-elevation stakes (~<400 m a.s.l.) showed relatively negative (out of
41 phase) correlation and higher elevated stakes relatively positive (in phase) eigenvector
42 correlation values with EOF2. Such relatively negative and positive eigenvector correlation
43 values were present where the surface of MG constituted of exposed glacier ice or snow cover,
44 respectively. The results from this study show how EOF analyses can provide robust information
45 on spatiotemporal patterns of glacier mass-balance. Understanding such detailed variabilities in
46 mass-balance on a Greenlandic glacier is of interest because a fifth of the Arctic contribution
47 from glaciers and ice caps to sea-level rise originated from Greenland.

48

49

50

51 **Keywords** Empirical Orthogonal Function analysis; Greenland; observations; mass-balance
52 stakes; Mittivakkat Gletscher

53 **1. Introduction**

54 At present, glaciers and ice caps are important contributors to eustatic sea-level rise (e.g.,
55 Marzeion et al. 2012; Gardner et al. 2013; Allison et al. 2015). Over the last several decades,
56 glaciers and ice caps in the Arctic have been observed to decrease in area and volume in
57 response to climate changes contributing to sea-level changes (Leclercq et al. 2011; Bjørk et al.
58 2012; Cogley 2012; Kargel et al. 2012; Marzeion et al. 2012; Zemp et al. 2015). Direct
59 glaciological surface mass-balance time series and glacier meteorology observations from local
60 glaciers (i.e. glaciers and ice caps surrounding the continental ice sheets; Weidick and Morris
61 1998) are scarce and sparsely distributed in Greenland. In total, less than 20 local glaciers in
62 Greenland have recorded mass-balance (B_a) observations covering different time periods since
63 1892-93 and to present (Machguth et al. 2016). At present, only five glaciers out of ~20,000
64 individual local glaciers in Greenland have ongoing annual glacier mass-balance observation
65 programs. This is a minor fraction of local glaciers in Greenland (Pfeffer et al. 2014; Radić et al.
66 2014), which cover a total area of $\sim 89,300 \pm 2,800 \text{ km}^2$ (Rastner et al. 2012). This lack of glacier
67 mass-balance observations leaves us with limited information about local glacier conditions in
68 Greenland and its contribution to sea-level changes. Local glaciers in Greenland are, for
69 example, less well-studied than the main ice sheet, so processes driving their change and their
70 sensitivity to climate variables are more unclear. However, it was recently stated by AMAP
71 (2017) that a fifth of the Arctic contribution from glaciers and ice caps to sea-level rise originates
72 from Greenland. It is, therefore, important to extract and generalize all relevant information
73 about these monitored glaciers.

74 Mittivakkat Gletscher (henceforth MG), located in Southeast Greenland on Ammassalik
75 Island, is Greenland's *only* peripheral glacier for which there exist long-term ongoing B_a records

76 continuously since the mass-balance year 1995/96 (Mernild et al. 2011). Even before this time,
77 B. Fristrup in 1933, 1958, and 1970 and B. Hasholt in 1986 and 1998 have demonstrated
78 relationships between climate-induced surface ablation and b_a variations and freshwater runoff
79 on MG (Fristrup 1970; Hasholt and Jakobsen 2008). The four other local glaciers in Greenland
80 with ongoing mass-balance monitoring programs are A. P. Olsen Iskappe (74.6°N, Zackenberg,
81 East Greenland; Larsen et al. 2012), Freya Gletscher (74.4°N, Clavering Island, East Greenland;
82 Hynek et al. 2014), Qaanaaq Gletscher, which is a part of Qaanaaq Iskappe (74.4°N, Qaanaaq,
83 Northwest Greenland; Sugiyama et al. 2014), and Qassinnguit Gletscher (64.1°N,
84 Nuuk/Kobberfjord, West Greenland; Abermann et al. 2014). The longest continuous
85 observational program beside the MG mass-balance program goes back to 2007 and is operated
86 by the Austrian Polar Research Institute on Freya Gletscher (Hynek et al. 2014; Machguth et al.
87 2016). A common characteristic for all ongoing local glacier mass-balance programs in
88 Greenland is that they show mean negative B_a for their period of observations.

89 As the MG mass-balance record started in 1995/96, MG is a valuable study site for
90 obtaining detailed understanding of trends in mass-balance (for both B_a and b_a) in Southeast
91 Greenland. On catchment-scale, MG also serves as an important site for studying the variability
92 of morphological characteristics (area, mean thickness, volume, surface slope, etc.) and ice
93 dynamics (Mernild et al. 2013a) and the climate sensitivity of local glaciers in Greenland
94 (Mernild et al. 2011, 2013b). Local glaciers in Southeast Greenland are influenced by air
95 temperature and precipitation changes following the oscillation in the Atlantic Multidecadal
96 Oscillation (AMO; Kaplan et al. 1998), where a relatively high temperature anomaly is in anti-
97 phase with a relatively low precipitation anomaly (during positive AMO), and vice versa (during
98 negative AMO) (Chylek et al. 2009; Mernild et al. 2012a). Since the end of the Little Ice Age

99 (~AD 1900), MG has undergone almost continuous retreat (Knudsen et al. 2008). MG has
100 reduced in area by 18 % (1986–2011), mean ice thickness by 22 % (1994–2012), volume by 30
101 % (1986–2011), and mean ice surface velocity by 30 %, which can be fully explained by the
102 dynamic effect of ice thinning (Mernild et al. 2013a; Yde et al. 2014). Further, MG has
103 undergone a surface elevation change where the vertical strain rate was able to compensate for
104 ~50 % of the surface elevation lowering due to the surface mass-balance (SMB) conditions
105 (Mernild et al. 2013a).

106 In this study, our aim is to address the knowledge gap in understanding the B_a variability,
107 with special focus on the variations between individual stake-observed b_a mass-balance
108 measurements. An improved understanding of long-term mass-balance variability is important to
109 emphasize the link between glacier changes, meteorology and albedo feedbacks. We do this by
110 analyzing a 19-year time series (1995/96–2013/14) of b_a data from 34 individual MG long-term
111 observation stakes. More specifically, we analyzed, mapped, and evaluated the patterns of both
112 temporal and spatial MG b_a variations using Empirical Orthogonal Functions (EOF). An EOF
113 analysis allows us to describe simultaneously how spatial patterns of b_a change over time among
114 the 34 stakes. It is possible to combine the EOF output with a cross-correlation analysis of local
115 and regional climate and geometric surface data to make hypotheses about the factors driving the
116 spatiotemporal patterns of b_a on MG. A detailed spatiotemporal mapping of b_a variation is
117 needed if we want to fully understand the factors influencing B_a conditions and the impact on the
118 hydrosphere in a “typical” Arctic landscape with a glacierized area, a downstream proglacial
119 valley and outwash plain, and a delta and coastal zone (Hasholt and Jakobsen 2008).

120 To our knowledge this is the first time in Greenland an EOF analysis has been conducted
121 on a local glacier scale to evaluate the spatiotemporal pattern in glacier b_a . MG mass-balance

122 data up to 2010/11 have earlier been published in Mernild et al. (2013a), although only the B_a
123 was analyzed. EOF analysis has previously been applied in glacier studies by Mair et al. (2002)
124 on Haut Glacier d'Arolla, Switzerland, who analyzed the spatiotemporal surface ice velocity
125 field. Also, Walters and Meier (1989) and Mernild et al. (2015a) have analyzed the large-scale
126 spatiotemporal variability of glacier B_a conditions in western North America and along the
127 Andes Cordillera to the sub-Antarctic islands, respectively. These analyses identified, for
128 example, correlations between B_a and large-scale atmospheric and oceanic indices.

129

130 **2. Study area**

131 Mittivakkat Gletscher formerly known as Midtluagkat Gletscher (26.2 km² in 2011);
132 65°41' N, 37°48' W) is located in the Ammassalik region, southeast Greenland (Figure 1). MG
133 extends from 180 to 880 m above sea-level (a.s.l.) (Knudsen et al. 2008), and from 1986–2011
134 the mean surface slope changed from 5.4 degree to 5.9 degree. Approximately ~19 % of MG (4.9
135 km²) had a slope between 6–10 degrees, ~20 % (5.2 km²) between 11–15 degrees, ~ and ~18 %
136 (4.8 km²) between 16–20 degrees (for other slope intervals, see Table 1, Figure 2). With regards
137 to aspect ~20 % (5.2 km²) of the surface are facing towards the west, whereas ~14 % (3.8 km²)
138 are facing northwestwards and ~13 % (3.5 km²) are facing southwestwards (for other slope
139 intervals, see Table 1, Figure 2). Since 1995, the ELA has risen from ~350 m a.s.l. to ~>880 m
140 a.s.l., with a mean ELA of ~750 m a.s.l. The ELA is the spatially averaged elevation of the
141 equilibrium line, defined as the set of points on the glacier surface where the net mass-balance is
142 zero. This ELA change has resulted in an average Accumulation Area Ratio (AAR) of 0.15
143 (Mernild et al. 2011). Hence, MG is significantly out of balance with the prevailing regional

144 climate and will likely lose at least 70 % of its current area and 80 % of its volume even in the
145 absence of further climate changes (Mernild et al. 2011).

146 Mean annual air temperature (MAAT) for the study period is -2.1°C (1993–2011) at
147 Station Nunatak (Hanna et al. 2012; Mernild et al. 2014a), and mean annual corrected
148 precipitation in the range of *c.* 1,400–1,800 mm water equivalent (w.e.) (1998–2006) (Mernild et
149 al. 2008b) (precipitation was corrected after Allerup et al. 1998, 2000). For Station Tasiilaq a
150 Danish Meteorological Institute (DMI) operated synoptic climate station located ~ 10 km
151 southeast of MG (Station Tasiilaq is not shown on Figure 1), MAAT and mean annual
152 precipitation sum changed (linear; both significant based on a linear regression *t*-test) $\sim 0.8^{\circ}\text{C}$
153 decade^{-1} and ~ -200 mm w.e. decade^{-1} , respectively (Hanna et al. 2012) . In this study, the term
154 ‘significant’ is only used when the relationship is statistically significant at the 5 % level or
155 better ($p \leq 0.05$).

156

157 **3. Methods**

158 *3.1 Mass-balance program*

159 The stake network used to measure the MG net annual balance (Figure 1) is based on the
160 direct glaciological method (Østrem and Brugman 1991); summer balance was calculated as the
161 difference between the measured net annual balance and the measured winter balance. As the
162 MG observations were started in the spring 1996 by measuring the winter accumulation along
163 transects and stakes were later drilled into the snow and ice during the early summer, there are no
164 direct observations of stake changes to determine net balance during the balance year 1995/96.
165 This made it possible to determine the summer balance in late-august 1996. The 1995/96 net

166 balance was determined as the winter balance subtracted the summer balance and not measured
167 directly at stakes.

168 Since 1996/97, mass-balance measurements from individual stakes were obtained
169 covering 16.3 km² of the main MG area, excluding the southeastern part of the glacier due to a
170 high density crevassed area and the northern part of the glacier due to logistical reasons. This
171 omission is not likely to bias the B_a results as the surface of these areas follows the general
172 hypsometric distribution of MG (Mernild et al. 2006). In total, 34 b_a stakes were used for this
173 study, where ~25 % have ≥ 15 annual observations during the period 1995/96–2013/14 and ~60
174 % have ≥ 10 (Figures 3 and 4). The locations of the stakes are shown in Figure 1 and cover the
175 elevation range of MG. Direct B_a observations are subject to uncertainties (where specifically
176 year 2002 seems to be underestimated, see further below). The methodological uncertainty of B_a
177 estimates on a single glacier is, according to Zemp et al. (2013), in the range of ± 340 mm w.e.
178 This uncertainty is due to a combination of measurement and analytic errors and has been added
179 to the data set.

180

181 *3.2 EOF analysis*

182 Empirical Orthogonal Function (EOF) analysis is a standard method in earth and marine
183 sciences for exploring spatio-temporal variation in a variable. It is a principle components
184 analysis applied to a data matrix organized by location (space) and time. The method has been
185 applied to glaciological analyses several times (e.g., Walters and Meier 1989; Mernild et al.
186 2015a). In this study, the focus is on the spatiotemporal variability in b_a .

187 Our approach to estimating the EOFs implements Data Interpolating Empirical
188 Orthogonal Functions (DINEOF; Beckers and Rixon 2003) because our data are ‘gappy’ with

189 missing data in various years at various stakes. Our use of DINEOF via the R ‘sinkr’ package
190 (<https://github.com/marchtaylor/sinkr>) fills gaps by iteratively decomposing the data field via
191 singular value decomposition until a best solution is found as compared to a subset of reference
192 values (Beckers and Rixon 2003; Taylor et al. 2013). We further extended the approach by
193 interpolating and estimating the EOFs for our data 50 times and using the mean of these. This is
194 because the interpolation process involves randomization and permutation.

195 As in any ordination technique, the major axes (e.g., EOF1 and EOF2) represent
196 independent collections of information on the variable of interest, and in this case, variations in
197 b_a in space and time. The EOF analysis captures variations in b_a simultaneously in time and space
198 (Figure 4). The significance of the variations captured by each EOF can be evaluated several
199 ways. These tools are designed to reveal how many major axes of variations there are in the data.
200 We relied on bootstrap randomization approach to estimate the significance (see
201 <https://github.com/marchtaylor/sinkr>).

202 The eigenvectors associated with such an analysis are linked to locations and thus reveal
203 the influence of different geographic locations on the summarized mass-balance patterns and
204 further allow analyses of meteorological covariates linked to the EOFs. All data were centered
205 around zero and scaled to unit variance (Mernild et al. 2015a).

206 We first examined the eigenvectors (loadings) of the first EOF, which showed how this
207 major axis of spatiotemporal variation in b_a varies among stake locations. This provides a
208 graphical visual summarization of the geographic patterns of temporal variation in b_a . The
209 second assessment involved exploring how these correlations among sites and EOF varied
210 regarding to site-specific characteristics such as elevation, slope, and aspect. The third
211 assessment involved relating the temporal trends in EOFs to observed temporal trends in

212 meteorological surface conditions. These trends include: i) observed MAAT (September through
213 August; following the mass-balance year) and mean summer surface air temperature (June
214 through August) from Station Nunatak; ii) observed MAAT, mean summer temperature, and
215 winter precipitation sum (September through May) from Station Tasiilaq, and iii) the observed
216 mean MG glacier-wide albedo.

217 The surface albedo is defined as the reflected fraction of incoming solar shortwave
218 radiation (e.g., Dumont et al. 2012) and is a parameter that governs energy availability for snow
219 and ice surface ablation, and subsequently variabilities in b_a conditions. The mean MG glacier-
220 wide surface albedo was estimated for a 16-day composite at the end of the mass-balance year
221 period (27/28 July–12/13 August; 2000–2013), derived from the MODerate Imaging
222 Spectroradiometer (MODIS MCD43A3) albedo product. For verification and technical details
223 about the MODIS MCD43A3 MG albedo product, see Mernild et al. (2015b).

224 For estimation of MG surface slope and aspect a digital elevation model (DEM) was
225 extracted from the Advanced Spaceborne Thermal Emission and Reflection Radiometer
226 (ASTER) Global Digital Elevation Model Version 2 (GDEM v2) (based on the best observations
227 between 2000 and 2010), with a vertical average precision of ~12 m over Greenland (Tachikawa
228 et al. 2011). The vertical error was expected to be closer to the GDEM v2 standard ± 8.7 m
229 precision due to the gentle slope (<10 degrees) of the MG surface (Table 1) from where the
230 measurements were taken (Tachikawa et al. 2011). The lateral error associated with GDEM v2 is
231 a little more than half a pixel (17 m). The ASTER GDEM v2 is a product of the US Ministry of
232 Economy, Trade, and Industry and NASA.

233

234 **4. Results and discussion**

235 *4.1 Variations in B_a observations*

236 In Figure 5, the MG B_a time series are shown. On average since 1995/96, annual B_a was -
237 1.00 ± 0.70 m water equivalent (w.e.) (where \pm equals one standard deviation), indicating a
238 cumulative mass-loss of 19 m w.e. (Figure 5). The MG B_a loss has on average changed (linear)
239 by -0.06 m w.e. yr^{-1} (significant; $r^2 = 0.26$, where r^2 is the square of the linear correlation
240 coefficient). Overall, in comparison to the other local glacier mass-balance programs in
241 Greenland (even though different time periods were compared), the mean annual B_a were
242 negative for all observed glaciers: -0.55 ± 0.56 m w.e. Freya Gletscher (2007/08–2013/14)
243 (Hynek et al. 2014), -0.40 ± 0.56 m w.e. Qaanaaq Gletscher (2012/13–2014/15) (Sugiyama et al.
244 2014), and -0.17 ± 0.34 m w.e. Qassinnguit Gletscher (2012/13–2014/15) (Abermann et al.
245 2014). Data were not available for A. P. Olsen Iskappe, as these data are too poorly constrained
246 (pers. com., M. Citterio, September 2014). The available observed mean B_a conditions indicate a
247 ‘snap-shot’ in time for various periods, where a mean negative B_a not only is a local phenomenon
248 at MG, but present at other mass-balance observed glaciers in SE, NE, NW, and W Greenland.

249 In 2010/11, the B_a at MG was at a record setting -2.45 m w.e. This was more than two
250 standard deviations (-2σ ; Figure 5) below mean. In both 2004/05 and 2009/10, B_a was more than
251 one standard deviation below mean (-1σ), and in 1995/96 and 2002/03 more than one standard
252 deviation above mean ($+1\sigma$). These deviations were highly dominated both by relatively high
253 mean summer temperature conditions and subsequently high ablation rates for 2004/05, 2009/10,
254 and 2010/11 or enhanced winter precipitation conditions causing high accumulation rates for
255 1995/96 and 2002/03. Annual and seasonal variabilities in surface air temperature have in
256 general an impact on the snow and firm temperature conditions (on the cold content), as
257 temperature changes propagate into the snow and firm (e.g., Cuffey and Patterson 2010).

258 Therefore, high MAAT likely indicates a relatively lower end of winter season (May 31) snow
259 cold content and subsequently contributing to an early start of the melt season.

260 When B_a was either below (2004/05, 2009/10, and 2010/11) or above one standard
261 deviation (1995/96 and 2002/03) between 66–100 % of the individual stake b_a observations had
262 values that were below or above one standard deviation, respectively. For the remaining 14
263 years, B_a was within one standard deviation. Overall for the observation period, changes in
264 glacier winter balance (B_w) and summer balance (B_s) explain 59 % and 90 % of the variability in
265 B_a (both significant; not shown), respectively. B_w and B_s were observed in 13 out of 19 years.

266 During the period 2004/05–2013/14, for example, seven of the highest recorded B_a losses
267 have occurred. During the past five years three of those losses were recorded in 2010/11,
268 2009/10 (-2.16 m w.e.), and 2011/12 (-1.63 m w.e.) (Figure 5). In terms of the mean surface
269 summer air temperature, the period 2004/05–2013/14 had six and seven of the highest values
270 observed at Station Nunatak and Station Tasiilaq, respectively (not shown). For Station Tasiilaq,
271 the period 2004/05–2013/14 also included seven of the driest winters recorded (not shown),
272 indicating that the climate in the MG region both got warmer and drier at the same time
273 (Cappelen 2015; Mernild et al 2012a).

274

275 *4.2 Variations in b_a observations*

276 The spatial distribution of mean MG observed b_a 1996/97–2013/14 is illustrated on
277 Figure 6a. Observed mean b_a values were lowest \sim -3.0 m w.e. at the lowest MG elevations close
278 at the margin (180 m a.s.l.) and \sim -0.5 m w.e. at the highest elevations (\sim 650 m a.s.l.), indicating
279 net ablation everywhere on the glacier. The mean annual b_a value of -1.0 m w.e. was observed at
280 \sim 500 m a.s.l., whereas mean b_a lower than -1σ (-1.7 m w.e.) and -2σ (-2.4 m w.e.) were observed

281 at elevations lower than ~400 m a.s.l. and ~300 m a.s.l., respectively (Figure 6a). The spatial and
282 longitudinal distributions of observed b_a variability (1σ) are illustrated in Figures 6b and 6e,
283 respectively, indicating that the temporal variability in b_a increased in value with increasing
284 elevation until 300–400 m a.s.l. Above this elevation the variability in b_a decreased slightly. In
285 the frontal area below 200 m a.s.l., the mean b_a standard deviation was 0.48 m w.e. and above
286 600 m a.s.l. it was 0.77 m w.e. The highest temporal variability of 0.85–0.88 m w.e. was present
287 at elevations between 300–600 m a.s.l. (Figure 6e). This peak in b_a variability at elevations
288 between 300–600 m a.s.l. along the central part of the glacier was likely identical to the average
289 ascent of the ELA over the observation period (Mernild et al. 2015b), probably because the
290 variability in b_a was influenced by the combined effects of changes in winter and summer
291 meteorological conditions. This elevation range (300–600 m a.s.l.) was also the area, where the
292 greatest change (-0.25) in the observed end of mass-balance year albedo occurred, identifying
293 this zone as an important surface cover and albedo transitional zone – an ELA zone (Mernild et
294 al. 2015b). The lowest variations in b_a together with the lowest changes in surface albedo both
295 occurred where MG was either snow covered at the end of the mass-balance year (in the high-
296 elevation accumulation zone) or constituted of exposed glacier ice (in the low-elevation ablation
297 zone). Hence, in case the variability in b_a followed the -1σ or $+1\sigma$ variability for a specific year,
298 b_a values in the frontal area would be as low as ~-3.5 m w.e. and at approximately 525 m a.s.l. ~-
299 1.8 m w.e. for -1σ (Figure 6c), and ~-2.6 m w.e. and ~0 m w.e. (identical with the location of the
300 ELA) for $+1\sigma$ (Figure 6d), respectively. In other words, b_a followed the upper and lower
301 boundaries of the longitudinal profile as illustrated in Figure 6e.

302

303 *4.3 b_a observations and EOF variance analysis*

304 In Figure 3, the annual observed b_a time series are shown for all 34 individual stakes on
305 MG. Overall, the variability in the b_a time series occurred both for each individual time series
306 and between the annual stake values. For some years such as 2002/03 ($\sigma = 0.45$ m w.e.), 2005/06
307 ($\sigma = 0.60$), and 2010/11 ($\sigma = 0.37$) marked with blue colored squares in Figure 3, the b_a spatial
308 variability was relatively low compared to other years 2000/01 ($\sigma = 1.04$), 2001/02 ($\sigma = 1.10$),
309 and 2012/13 ($\sigma = 1.09$) marked with red colored circles. This indicates that for the first three
310 highlighted years relatively homogeneous b_a conditions and a low b_a gradient existed, and
311 opposite for the last three highlighted years. The years with relatively negative B_a (Figure 5)
312 were the years with relatively low spatial variability in b_a (i.e., relatively homogeneous b_a
313 conditions, Figure 3), and opposite for years with less negative or positive B_a ($r^2 = 0.43$,
314 significant).

315 In Figure 7, we report on two major axes (modes) estimated from our EOF analysis of
316 spatiotemporal variation: EOF1 and EOF2 representing 80 % (significant) and 6 %
317 (insignificant) of the explained variance, respectively. The temporal and spatial variability in
318 EOF1 and EOF2 are illustrated in Figures 7 and 8, respectively. Regarding EOF1, we show a
319 five-year running mean smoothing line that increased over the time-period, being negative until
320 2003 and positive thereafter (Figure 7). For EOF2 the five-year running mean smoothing line
321 oscillated with an approximately six-year frequency. EOF2 was negative during the periods
322 1995–1999, 2003–2006, and 2009–2012 and positive during the periods 1999–2003, 2006–2009,
323 and after 2012. Hence, the EOF2 five year running mean smoothing line was more complex than
324 the EOF1 pattern.

325 Both the temporal EOF1 and EOF2 patterns were associated with individual eigenvectors
326 for each individual stake (Figure 8). For EOF1, the bar-plot in Figure 8 illustrates negative

327 values for *all* stakes, indicating that EOF1 was capturing increasing mass loss at all stakes and
328 therefore decreasing annual B_a loss. These negative correlations emphasize that variations in
329 mass-loss were uniformly distributed in space and time at all stakes (Figures 8a and 9a).

330 We found that EOF1 showed a significant correlation with Station Nunatak mean
331 summer air temperature and glacier-wide albedo (Figure 10 and Table 2). However, we also
332 noted that values at year 2002 were a statistical outlier (due to an underestimation of measured
333 b_a). As an example, if we ignore the year 2002 values EOF1 was correlated with MAAT and
334 mean summer air temperature from both Station Nunatak and Station Tasiilaq and observed
335 mean glacier-wide albedo, but not winter precipitation sum from Station Tasiilaq (Figure 11 and
336 Table 2). We suggest that EOF1 strongly reflected variability in air temperature conditions and
337 albedo, rather than variability in precipitation conditions and topographic conditions. None of the
338 correlations to precipitation at both Station Nunatak and Station Tasiilaq were significant (Table
339 2). We suggest that this is because precipitation in Greenland varies according to the topography
340 and the patterns of weather systems and even within short distances precipitation is likely
341 explained by prevailing wind circulation e.g., katabatic winds draining downslope from the ice-
342 sheet interior, distance from the oceanic moisture source and the orographic effect of near-
343 coastal mountains. The latter is especially important in Southeast Greenland (e.g., Hansen et al.
344 2008) and in the area of MG, where the mean corrected annual precipitation varies from ~1,250
345 mm w.e. (1999–2006) (uncorrected ~900 mm w.e.) at Station Tasiilaq to ~1,850 mm w.e. at
346 Station Nunatak (1999–2006) (Mernild et al. 2008b, 2015c).

347 Station Tasiilaq is located around 10 km southeast of MG and highly influenced by
348 maritime climate conditions, having a mean monthly air temperature range of 10–15°C
349 (Cappelen et al. 2015). In comparison, Station Nunatak was influenced by coastal climate

350 conditions, having a mean monthly air temperature range of 15–25°C (Mernild et al. 2008b). At
351 MG the B_a variability is significantly correlated with variabilities in both maritime and coastal
352 climate conditions (for definitions of maritime and coastal climate conditions, see Przybylak
353 2003). It therefore seems very likely that similar variabilities in B_a may occur for other glaciers
354 located within maritime and coastal climate conditions in Southeast Greenland. Due to the
355 significant correlation between MG B_a and observed air temperature both at Station Nunatak and
356 Station Tasiilaq – two stations located in different climate conditions –, we propose that
357 variability in B_a is not only a local phenomenon. Mernild et al. (2011) found that MAAT time
358 series from Southeast Greenland’s coastal DMI stations were significantly correlated with
359 MAAT time series from Station Tasiilaq. These data further suggest that B_a variability at MG,
360 which has been driven largely by surface air temperature variabilities, is representative for mass-
361 balance variations on a regional scale, which includes many hundreds of local glaciers. In
362 support of this statement, the trends in glacier terminus recession at MG and mass-balance
363 conditions are on average similar to glacier terminus recessions for land-terminating glaciers in
364 the Ammassalik region (Mernild et al. 2012b) and overall for land-terminating glaciers in
365 Southeast Greenland (Bjørk et al. 2012), and to simulated mass-balance conditions in the
366 Ammassalik region (Mernild et al. 2014b), respectively.

367 In contrast to the EOF1 dataset, the EOF2 pattern was complex and showed a more
368 spatial variable pattern with in total 11 (shown with light gray color) out of 34 stakes (~33 % of
369 the stakes) being in phase with EOF2 and 23 stakes (~67 % of the stakes) being out of phase
370 with EOF2 (dark gray; Figure 8b). While our bootstrap analysis indicates that the 6 % of
371 variation captured by EOF2 is not significant given the current set of data, we explore it because

372 the EOF2 pattern was complex and showed a more spatial variable pattern than the EOF1
373 dataset; we note these thus represent hypotheses about more localized patterns in b_a .

374 Surface elevation, slope, and aspect explained none of the b_a site-specific correlations
375 with EOF1, but they explained variation in the spatial component of EOF2 (Figures 9a–9c). We
376 suggest that the 11 stakes being in phase with EOF2 may have different mean geometrical
377 surface terrain features such as different mean surface slope and aspect than the other 23 stakes
378 in the mass-balance network. In general, we found that the 11 stakes being in phase with EOF2
379 likely had lower mean surface slope than the other 23 stakes being out of phase with EOF2 (see
380 also Figure 9b). For these 11 stakes, the mean surface slope was 8.5 degrees, whereas the mean
381 slope at the other 23 stakes was 11.0 degrees (significant not equal). Further, our analysis
382 indicates that the stakes being in phase with EOF2 mainly had south facing aspects; whereas
383 stakes being out of phase with EOF2 mainly had west and north facing aspects (see also Figure
384 9c). Even though the EOF2 pattern probably can be explained by the variability in surface
385 conditions – by the mean surface slope and/or aspect, the more general EOF1 pattern seemed to
386 be dominated by other controls than surface characteristics such as variations in meteorological
387 conditions.

388 Further, EOF2 indicated a general eigenvector correlation pattern related to elevations on
389 MG, where low-elevated stakes ($\sim < 400$ m a.s.l.) showed relatively negative (out of phase)
390 eigenvector correlation values and higher elevated stakes relatively positive (in phase)
391 eigenvector correlation values (Figure 9a). Such relatively negative and positive eigenvector
392 correlation values were present where MG either constituted of exposed glacier ice in the low-
393 elevated ablation zone or snow cover in the high-elevated accumulation zone during b_a
394 observations. Also, these patterns were likely related to changes in both MG snow cover duration

395 and the occurrence of frequent air temperature inversion on the lower part of MG (~<300 m
396 a.s.l.): Inversion and sea breezes associated with the adjacent relatively low temperature and
397 frequently ice-choked fjords and oceans (Mernild and Liston 2010). Observations indicate that
398 air temperature inversion is to be present 84 % of the time, and essential for accumulation and
399 surface ice melt conditions (Mernild and Liston 2010). Therefore, in general these EOF2 stake
400 eigenvector correlations likely indicated a change from eigenvectors being out of phase to
401 eigenvector being in phase with increasing elevation, even though minor fluctuations in
402 eigenvector correlations occurred due to variations in both surface slope and aspect (even within
403 a distance less than a few hundred of meters). The EOF2 correlation values emphasize that
404 variations in mass-loss were heterogeneously distributed (insignificant) in space and time at the
405 MG stakes.

406 An understanding of such MG EOF correlations – its variability to changes in climate and
407 surface conditions – is of interest for different purposes because local glaciers in Greenland are
408 less well-studied than the Greenland Ice Sheet, but also for mass-balance upscaling proposes to
409 regions from where no glacier mass-balance observations are available.

410

411 **5. Conclusions**

412 Our findings show that in 14 out of 19 years, B_a was within one standard deviation with a
413 mean annual loss of -1.00 ± 0.70 m w.e., a change of -0.06 m w.e. yr^{-1} during a period of climate
414 warming and drying, following the variability in AMO (Mernild et al. 2012a). Relatively
415 negative MG B_a equal low spatial variability in b_a . A change in B_a indicates that the greatest
416 variability in b_a occurred for stakes located between 300–600 m a.s.l. and is likely related to the
417 ascent of the ELA.

418 The EOF analysis is a robust way of obtaining spatiotemporal information on glacier
419 mass-balance patterns. The use of a statistical EOF variance analysis suggests that observed b_a
420 on MG in time and space can be summarized by a single major axis of variation EOF1
421 representing 80 % (significant) of the explained variance. Further, EOF1 emphasizes variations
422 in b_a related to variations in albedo and surface air temperature observations from nearby
423 maritime and coastal stations. However, we also explore the second major axis, which explained
424 6 %, because it suggests possible localized geographic effects on b_a linked to surface conditions
425 associated with slope and aspect. Our EOF calculations are crucial for our understanding of
426 spatiotemporal mass-balance variabilities and for mass-balance upscaling possibilities in
427 Greenland because variabilities in b_a are influenced strongly by variabilities in summer air
428 temperature and MAAT and mean glacier-wide observed albedo, and insignificant against
429 surface characteristics such as slope and aspect. Additionally, it is crucial for our understanding –
430 in case of upscaling to regions with no observations – because we have few mass-balance
431 observations from local glaciers in Greenland.

432

433 **Acknowledgements**

434 We thank Japan Society for Promote Science (JSPS) for support, under grant agreement
435 No. S17096. Also, we thank InterAct for support, under the project: ALBICE, where the research
436 leading to these results has received funding from the European Union’s Horizon 2020 project
437 INTERACT, under grant agreement No. 730938. We thank the all the people who have
438 participated in the Mittivakkat Gletscher mass-balance fieldwork over the years. Finally, we
439 thank the Danish Meteorological Institute for providing World Meteorological Organization

440 synoptic meteorological data from Tasiilaq, and University of Copenhagen for providing
441 meteorological data from and around the Mittivakkat Gletscher.

442

443

444

445

446

447

448

449

450

451

452

453

454

455

456

457

458

459

460

461

462

463

464

465

466

467

468

469

470 **References**

471 Abermann, J., van As, D., Petersen, D., and Nauta, M. 2014. A new glacier monitoring site in
472 West Greenland. *Abstract AGU Fall meeting*, December 2014.

473
474 Allerup, P., Madsen, H., and Vejen, F. 1998. Estimating true precipitation in arctic areas. In
475 *Proceedings of the Nordic Hydrological Conference*. Helsinki: Nordic Hydrological Programme
476 Report, 44, 1–9.

477
478 Allerup, P., Madsen, H., and Vejen, F. 2000. Correction of precipitation based on off-site
479 weather information. *Atmos. Res.* 53, 231–250.

480
481 Allison, I., Colgan, W., King, M., and Paul, F. 2015. Ice Sheets, Glaciers, and Sea Level
482 (Chapter 20). In *Snow and Ice-Related Hazards, Risks, and Disasters*, (ed.) Haeberli, W.,
483 Whiteman, C., and Shroder, J. F., Elsevier, Amsterdam, 713–747.

484
485 AMAP, 2017. Snow, Water, Ice and Permafrost. Summary for Policy-makers. Arctic Monitoring
486 and Assessment Programme (AMAP), Oslo, Norway. 20 pp

487
488 Beckers, J.-M. and Rixen, M. 2003. EOF Calculations and Data Filling from Incomplete
489 Oceanographic Datasets. *Journal of Atmospheric and Oceanic Technology*, 20(12), 1839–1856.

490
491 Bjørk, A. A., Kjær, K. H., Korsgaard, N. J., Khan, S. A., Kjeldsen, K. K., Andresen, C. S., Box,
492 J. E., Larsen, N. K., and Funder, S. 2012. An areal view of 80 years of climate-related glacier
493 fluctuations in Southeast Greenland. *Nature Geoscience*, 5, 427–432.

494
495 Cappelen, J. 2015. Greenland - DMI Historical Climate Data Collection 1784-2014. Technical
496 Report DMI, 15-04, pp. 97. www.dmi.dk/fileadmin/user_upload/Rapporter/TR/2015/tr15-04.pdf

497
498 Chylek, P., Folland, C., Lesins, G., Wang, M. and Dubey, M. 2009. Arctic air temperature change
499 amplification and the Atlantic multidecadal oscillation. *Geophysical Research Letter*, 36,

500 L14801.

501
502 Cogley, J. G. 2012. The future of the world's glaciers. *The Future of the World's Climate*, 2nd
503 ed., A. Henderson-Sellers and K. McGuffie, Eds., Elsevier, 205–218, doi:10.1016/B978-0-12-
504 386917-3.00008-7.
505
506 Cuffey, K. M. and Patterson, W. S. B. 2010 *The Physics of Glaciers*. Fourth Edition. Oxford, pp.
507 693.
508
509 Dumont, M., Gardelle, J., Sirguey, P., Guillot, A., Six, D., Rabatel, A., and Arnaud, Y. 2012.
510 Linking glacier annual mass balance and glacier albedo retrieved from MODIS data. *Cryosphere*,
511 6, 1527–1539, doi:10.5194/tc-6-1527-2012.
512
513 Fristrup, B. 1970. New Geographical Station in Greenland. *Geografisk Tidsskrift-Danish Journal*
514 *of Geography*, 69, 199–203.
515
516 Gardner, A. S., and Coauthors 2013. A reconciled estimate of glacier contributions to sea level
517 rise: 2003 to 2009. *Science*, 340, 852–857, doi:10.1126/science.1234532.
518
519 Hanna, E., Mernild, S. H., Cappelen, J., and Steffen, K. 2012. Recent warming in Greenland in a
520 long-term instrumental (1881–2012) climatic context. Part 1: Evaluation of surface air
521 temperature records. *Environmental Research Letters*, 7, 045404, doi:10.1088/1748-
522 9326/7/4/045404.
523
524 Hansen, B. U., Sigsgaard, C., Rasmussen, L., Cappelen, J., Hinkler, J., Mernild, S. H., Petersen,
525 D., Tamstorf, M., Rasch, M. and Hasholt, B. 2008. Present Day Climate at Zackenberg.
526 *Advances in Ecological Research*, 40, 115–153.
527
528 Hasholt, B., and Jakobsen, B. H. 2008. 75 years of research at the Sermilik Station: 1933–2008.
529 *Geografisk Tidsskrift-Danish Journal of Geography*, 108, 1–4.
530
531 Hynek, B., Weyss, G. Binder, D., and Schöner, W. 2014. Mass Balance of Freya Glacier,

532 2007/2008-2012/2013. *Pangea*, doi:10.1594/PANGAEA.831035.
533
534 Kaplan, A., Cane, M., Kushnir, Y., Clement, A., Blumenthal, M., and Rajagopalan, B. 1998.
535 Analyses of global sea surface temperature 1856–1991. *Journal of Geophysical Research*, 103,
536 18,567–18,589.
537
538 Kargel, J. S., Ahlstrøm, A. P., Alley, R. B., Bamber, J. L., Benham, T. J., Box, J. E., Chen, C.,
539 Christoffersen, P., Citterio, M., Cogley, J. G., Jiskoot, H., Leonard, G. J., Morin, P., Scambos,
540 T., Sheldon, T., and Willis, I. 2012. Brief communication Greenland’s shrinking ice cover:
541 “fast times” but not that fast. *The Cryosphere*, 6, 533–537.
542
543 Knudsen, N. T., Nønborg, P., Yde, J. C., Hasholt, B., and Heinemeier, J. 2008. Recent marginal
544 changes of the Mittivakkat Glacier, Southeast Greenland and the discovery of remains of
545 reindeer (*Rangifer tarandus*), polar bear (*Ursus maritimus*) and peaty material. *Geografisk*
546 *Tidsskrift-Danish Journal of Geography*, 108(1), 137–142
547
548 Leclercq, P. W., Oerlemans, J., and Cogley, J. G. 2011. Estimating the glacier contribution to
549 sea-level rise for the period 1800–2005. *Surv. Geophys.*, 32, 519–535, doi:10.1007/s10712-011-
550 9121-7.
551
552 Larsen, S. H., Citterio, M., Hock, R., and Ahlstrom, A. P. 2012. Mass and surface energy
553 balance of A.P. Olsen ice cap, NE Greenland, from observations and modeling (1995–2011).
554 *Abstract AGU Fall meeting*, C23B-0660.
555 .
556
557 Machguth, H., Thomsen, H. H., Weidick, A., Abermann, J., Ahlstrom, A. P., Andresen, M. L.,
558 Andersen, S. B., As, D. van, Boeggild, C. E., Box, J. E., Braithwaite, R. J., Citterio, M., Clement,
559 P., Colgan, W., Fausto, R. S., Gleie, K. Hasholt, B., Hynek, B., Knudsen, N. T., Mernild, S. H.,
560 Oerter, H., Olesen, O. B., Steffen, K., Stober, M., Sugiyama, S., and van de Wal, R. S. W. 2016.
561 A comprehensive database of Greenland surface mass balance observations from the ice sheet
562 ablation area and the local glaciers. Accepted *Journal of Glaciology*.

563
564 Mair, D., Nienow, P., Sharp, M., Wohlleben, T., and Wills, I. 2002. Influence of subglacial
565 drainage system evolution on glacier surface motion: Haut Glacier d'Arolla, Switzerland. *Journal*
566 *of Geophysical Research – Solid Earth*, 107(B8), 1-13, 10.1029/2001JB000514.
567
568 Marzeion, B., Jarosch, A. H., and Hofer, M. 2012. Past and future sea-level change from the
569 surface mass balance of glaciers. *Cryosphere*, 6, 1295–1322, doi:10.5194/tc-6-1295-2012.
570
571 Mernild, S. H., Hanna, E., McConnell, J. R., Sigl, M., Beckerman, A. P., Yde, J. C., Cappelen, J.,
572 and Steffen, K. 2015c. Greenland precipitation trends in a long-term instrumental climate context
573 (1890–2012): Evaluation of coastal and ice core records. *International Journal of Climatology*,
574 35, 303–320, doi:10.1002/joc.3986.
575
576 Mernild, S.H., Hanna, E., Yde, J.C., Cappelen, J., and Malmros, J.K. 2014a. Coastal Greenland
577 air temperature extremes and trends 1890–2010: annual and monthly analysis. *International*
578 *Journal of Climatology*, 34, 1472–1487, doi:10.1002/joc.3777.
579
580 Mernild, S. H., Hansen, B. U., Jakobsen, B. H., and Hasholt, B. 2008b. Climatic conditions at the
581 Mittivakkat Glacier catchment (1994–2006), Ammassalik Island, SE Greenland, and in a 109
582 years term perspective (1898–2006). *Geografisk Tidsskrift-Danish Journal of Geography*,
583 108(1): 51–72.
584
585 Mernild, S. H. and G. E. Liston 2010. The influence of air temperature inversion on snow melt
586 and glacier surface mass-balance simulations, SW Ammassalik Island, SE Greenland. *Journal of*
587 *Applied Meteorology and Climate*, 49(1), 47–67.
588
589 Mernild, S. H., Liston, G. E., Hasholt, B., and Knudsen, N. T. 2006. Snow distribution and melt
590 modeling for Mittivakkat Glacier, Ammassalik Island, SE Greenland. *Journal of*
591 *Hydrometeorology*, 7, 808–824.
592

593 Mernild, S. H., Liston, G. E., and Hiemstra, C. A. 2014b. Northern Hemisphere glaciers and ice
594 caps surface mass balance and contribution to sea-level rise. *Journal of Climate*, 27(15), 6051–
595 6073, doi.org/10.1175/JCLI-D-13-00669.1.

596

597 Mernild, S. H., Knudsen, N. T., Hoffman, M. J., Yde, J. C., Lipscomb, W. L., Hanna, E.,
598 Malmros, J. K., and Fausto, R. S. 2013a. Volume and velocity changes at Mittivakkat Gletscher,
599 Southeast Greenland, 1994–2012. *Journal of Glaciology*, 59(216), 660–670,
600 doi:10.3189/2013JoG13J017.

601

602 Mernild, S. H., Knudsen, N. T., Lipscomb, W. H., Yde, J. C., Malmros, J. K., Jakobsen, B. H.,
603 and Hasholt, B. 2011. Increasing mass loss from Greenland’s Mittivakkat Gletscher. *The*
604 *Cryosphere*, 5, 341–348: doi:10.5194/tc-5-341-2011.

605

606 Mernild, S. H., Lipscomb, W. H., Bahr, D. B., Radić, V., and Zemp, M. 2013b. Global glacier
607 retreat: A revised assessment of committed mass losses and sampling uncertainties. *The*
608 *Cryosphere*, 7, 1565–1577, doi:10.5194/tc-7-1565-2013.

609

610 Mernild, S. H., Beckerman, A. P., Yde, J. C., Hanna, E., Malmros, J. K., Wilson, R., and Zemp,
611 M. 2015a. Mass loss and imbalance of glaciers along the Andes to the sub-Antarctic islands.
612 *Global and Planetary Change*, 133, 109–119: doi:10.1016/j.gloplacha.2015.08.009.

613

614 Mernild, S. H., Malmros, J. K., Yde, J. C., and Knudsen, N. T. 2012b. Multi-decadal marine and
615 land-terminating glacier retreat in Ammassalik region, Southeast Greenland. *The Cryosphere*, 6,
616 625–639, doi:10.5194/tc-6-625-2012.

617

618 Mernild, S. H., Malmros, J. K., Yde, J. C., Knudsen, N. T., Wilson, R., Hanna, E., Fausto, R. S.,
619 van As, D. 2015b. Albedo decline on Greenland’s Mittivakkat Gletscher. *International Journal*
620 *of Climatology*, 35, 2294–2307, doi: 10.1002/joc.4128.

621

622 Mernild, S. H., Seidenkrantz, M.-S., Chylek, P., Liston, G. E., and Hasholt, B. 2012a. Climate-
623 driven fluctuations in freshwater to Sermilik Fjord, East Greenland, during the last 4000 years.
624 *The Holocene*, 22(2), 155–164, doi:10.1177/0959683611431215.

625

626 Pfeffer, T. W., Arendt, A. A., Bliss, A., Bolch, T., Cogley, J. G., Gardner, A. S., Hagen, J.-O.,
627 Hock, R., Kaser, G., Kienholtz, C., Miles, E. S., Moholdt, G., Molg, N., Paul, F., Radić, V.,
628 Rastner, P., Raup, B. H., Ricj, J., Sharp, M. J., The Randolph Consortium, 2014. The
629 Randolph Glacier Inventory: a globally complete inventory of glaciers. *Journal of Glaciology*,
630 60(221), 537–552.

631

632 Przybylak, R. 2003. *The climate of the Arctic*. Kluwer Academic Publishers, Atmospheric and
633 Oceanographic Sciences Library 26, 270 pp.

634

635 Radić, V., Bliss, A., Beedlow, A. C., Hock, R., Miles, E., and Cogley, J. G. 2014. Regional and
636 global projection of twenty-first century glacier mass changes in response to climate scenarios
637 from global climate models. *Climate Dynamics*, 42, 37–58.

638

639 Rastner, P., Bolch, T., Mölg, N., Machguth, H., Le Bris, R., and Paul, F. 2012. The first
640 complete inventory of the local glaciers and ice caps on Greenland. *The Cryosphere*, 6, 1483–
641 1495, doi:10.5194/tc-6-1483-2012.

642

643 Sugiyama, S. Sakakibara, D., Matsuno, S., Yamaguchi, S., Matoba, S., and Aoki, T. 2014.
644 Initial field observations on Qaanaaq ice cap, northwestern Greenland. *Annals of Glaciology*,
645 55(66), 25–33.

646

647 Tachikawa, T. and 12 others (ASTER GDEM Validation Team) 2011. *ASTER Global Digital*
648 *Elevation Model Version 2 – summary of validation results, NASA Land Processes*. NASA
649 Distributed Active Archive Center, Joint Japan–US ASTER Science Team,
650 [http://www.jspacesystems.or.jp/ersdac/GDEM/ver2Validation/Summary_GDEM2_validation_re](http://www.jspacesystems.or.jp/ersdac/GDEM/ver2Validation/Summary_GDEM2_validation_report_final.pdf)
651 [port_final.pdf](http://www.jspacesystems.or.jp/ersdac/GDEM/ver2Validation/Summary_GDEM2_validation_report_final.pdf)

652

653 Taylor, M. H., Losch, M., Wenzel, M., and Schroeter, J. 2013. On the sensitivity of field
654 reconstruction and prediction using Empirical Orthogonal Functions derived from gappy data.
655 *Journal of Climate*, 26, 9194–9205.

656

657 Walters, R. A. and Meier, M. F. 1989. Variability of glacier mass balances in western North
658 America, in aspects of climate variability in the Pacific and the western Americas (ed. D. H.
659 Peterson), American Geophysical Union, Washington, D. C., doi: 10.1029/GM055p0365.

660

661 Weidick, A., and Morris, E., 1998. Local glaciers surrounding the continental ice sheets. In
662 Haeberli, W., Hoelzle, M., and Suter, S. (eds.), *Into the second century of world glacier*
663 *monitoring – prospects and strategies*. Paris: UNESCO. UNESCO Studies and Reports in
664 Hydrology, 56, 167–176.

665

666 Yde, J. C., Gillespie, M. K., Løland, R., Ruud, H., Mernild, S. H., de Villiers, S., Knudsen, N. T.
667 and Malmros, J. K. 2014. Volume measurements of Mittivakkat Gletscher, southeast Greenland.
668 *Journal of Glaciology*, 60(224), 1199-1207, doi: 10.3189/2014JoG14J047.

669

670 Zemp, M., Frey, H., Gartner-Roer, I., Nussbaumer, S. U., Hoelzle, M., Paul, F., Haeberli, W.,
671 Denzinger, F., Ahlstrom, A. P., Anderson, B., Bajracharya, S., Baroni, C., Braun, L. N., Caceres,
672 B. E., Casassa, G., Cobos, G., Davila, L. R., Granados, H. D., Demuth, M. N., Espizua, L.,
673 Fischer, A., Fujita, K., Gadek, B., Ghazanfar, A., Hagen, J. O., Holmlund, P., Karimi, N., Li, Z.,
674 Pelto, M., Pitte, P., Popovnin, V. V., Portocarrero, C. A., Prinz, R., Sangewar, C. V., Severskiy,
675 I., Sigurdsson, O., Soruco, A., Usubaliev, R., and Vincent, C. 2015: Historically unprecedented
676 global glacier decline in the early 21st century. *Journal of Glaciology*, 61(228), 745–762, doi:
677 10.3189/2015JoG15J017.

678

679 Zemp, M., Thibert, E., Huss, M., Stumm, D., Rolstad Denby, C., Nuth, C., Nussbaumer, S. U.,
680 Moholdt, G., Mercer, A., Mayer, C., Joerg, P. C., Jansson, P., Hynek, B., Fischer, A., Escher-
681 Vetter, H., Elvehøy, H. and Andreassen, L. M. 2013. Uncertainties and re-analysis of glacier
682 mass balance measurements. *The Cryosphere*, 7, 1227–1245.

683

684 Østrem, G. and Brugman, M. 1991: Glacier mass-balance measurements: a manual for field and
685 office work. NHRI Science Report 4. Environment Canada. National Hydrology Research
686 Institute, Saskatoon, Sask.

687

688

689

690

691

692

693

694

695

696

697

698

699

700

701

702

703

704

705

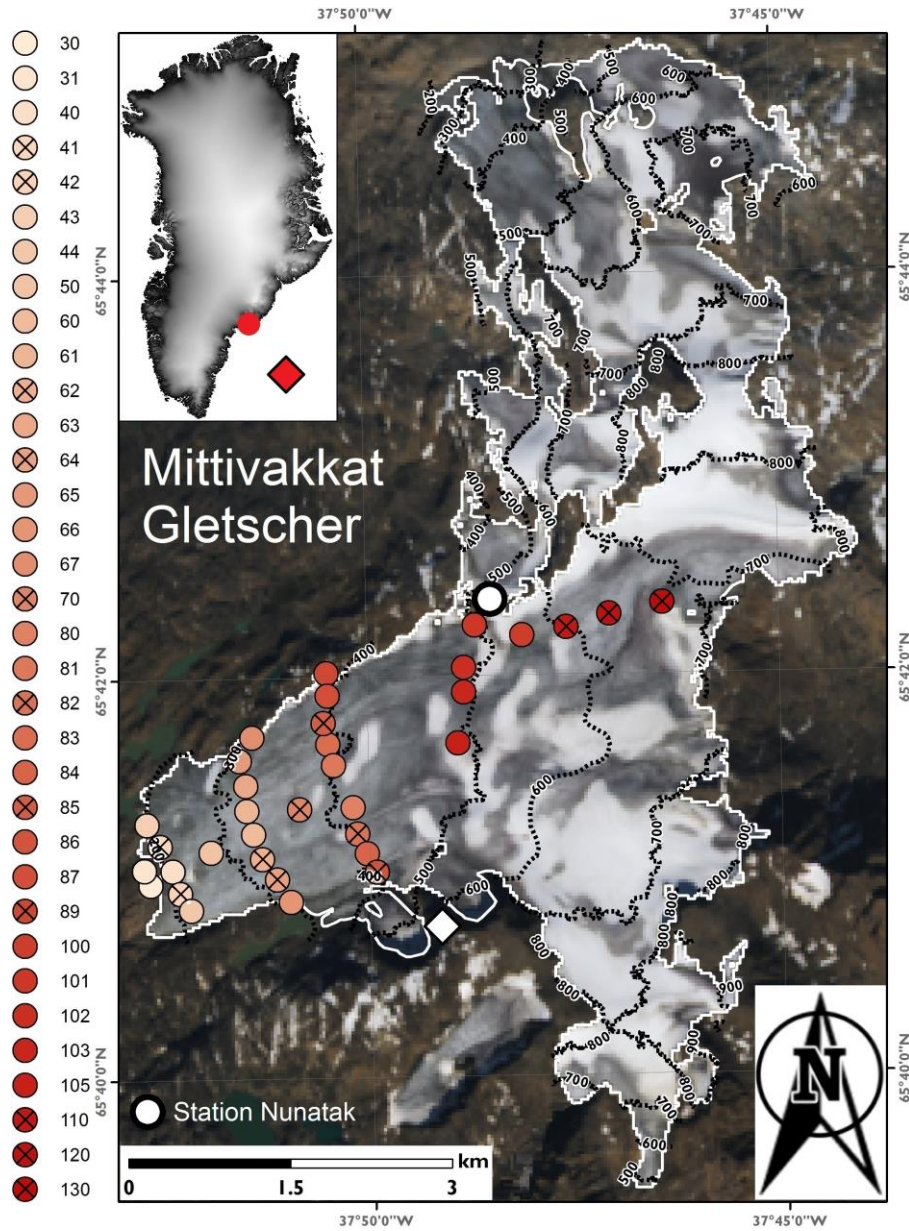
706

707

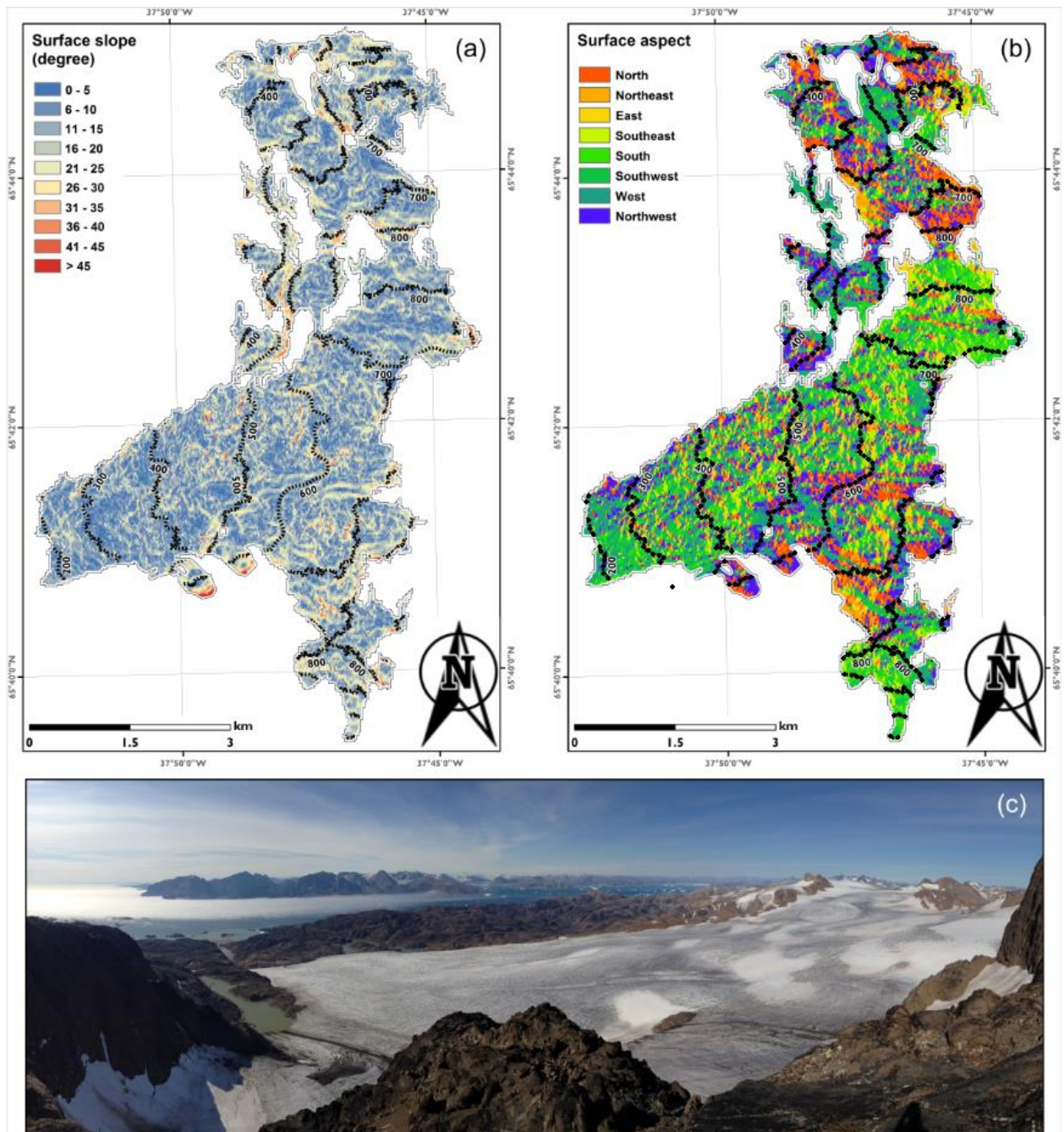
708

709

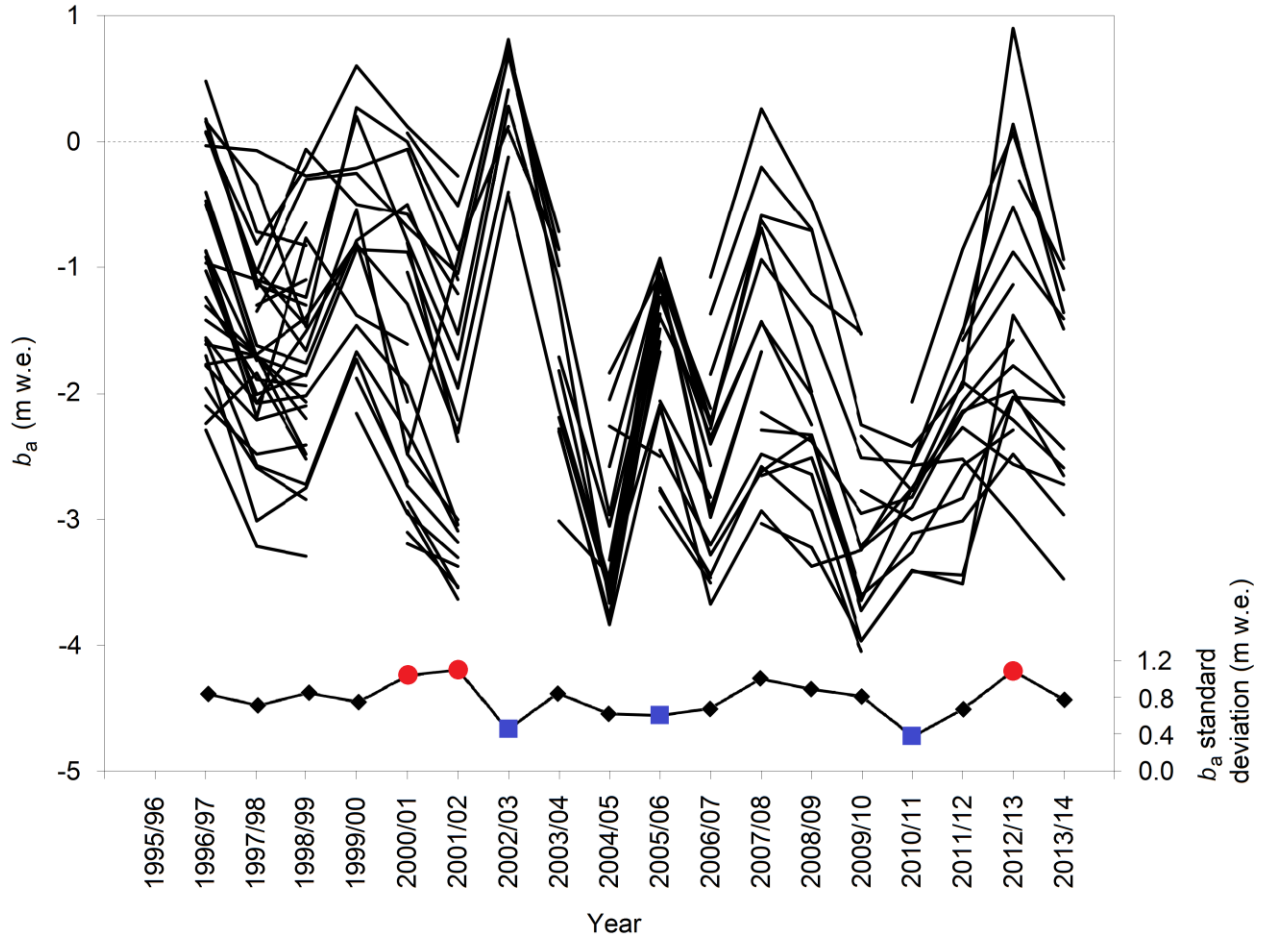
710



711
 712 **Figure 1:** Mittivakkat Gletscher (26.2 km² (2011); 65°41'N, 37°48'W) topographic map (100-m
 713 contour interval). The colored circles illustrate the 34 stake locations for the ongoing glacier
 714 mass-balance observation program, 1995/96–2013/14. The stake colors on the glacier surface
 715 correspond to the stake numbers illustrated to the left, where the low numbers correspond to the
 716 stakes at the low-elevation part of the glacier. Stakes in anti-phase for the EOF2 analysis are
 717 shown with a cross. Station Nunatak (515 m a.s.l.) is illustrated with a white circle. Station
 718 Tasiilaq is not included as it is located ~10 km southeast of the glacier. The white diamond
 719 indicates the location where the photo in Figure 2c was taken. Source: Landsat 8, OLI
 720 (Operational Land Imager), 7 August 2014.



721
 722 **Figure 2:** Mittivakkat Gletscher: (a) surface slope; (b) surface aspect; and (c) photo of the
 723 southwestern part of the glacier (the photo was taken looking north northwest, and in the
 724 background is Sermilik Fjord and the Greenland Ice Sheet, photo M. Lidström, August 2014).
 725 Area values for each slope and aspect interval are shown in Table 1. Surface slope and aspect is
 726 constructed based on the Advanced Spaceborne Thermal Emission and Reflection Radiometer
 727 (ASTER) Global Digital Elevation Model Version 2 (GDEM v2). The glacier margin outline is
 728 from 7 August 2014.



729

730 **Figure 3:** Time series of individual observed b_a time series from Mittivakkat Gletscher for the
 731 period 1996/97–2013/14, including calculated annual variability of b_a (at the bottom). The three
 732 maximum and minimum annual variabilities are marked with red circles and blue squares,
 733 respectively.

734

735

736

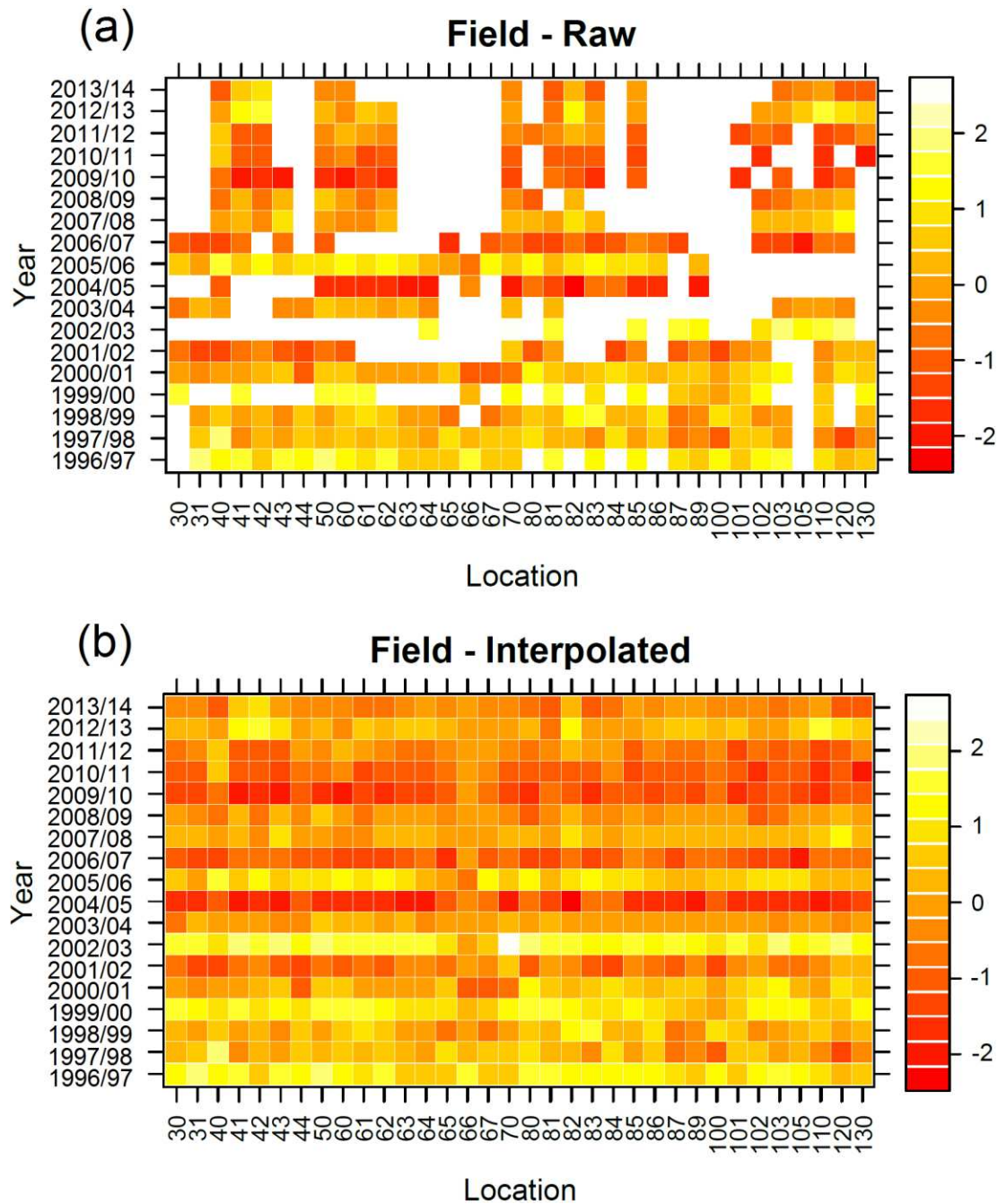
737

738

739

740

741



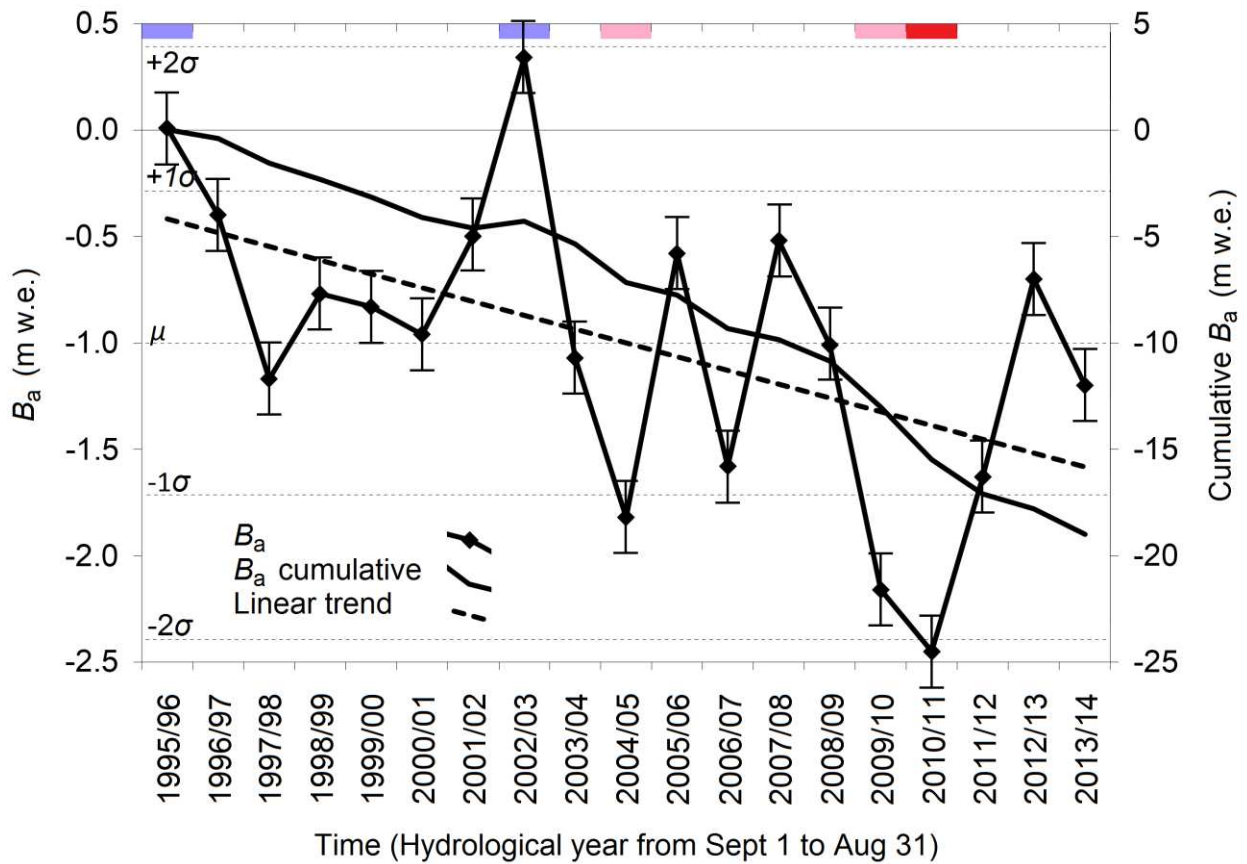
742

743 **Figure 4:** Space-time field (1996/97–2013/14) for Mittivakkat Gletscher, where the stake
 744 locations from left to right go from lowest stake numbers to highest stake number: (a) raw data
 745 field (the white squares equal no data): and (b) reconstructed data field. The reconstructed field is
 746 the mean of replicate reconstructions using the DINEOF method.

747

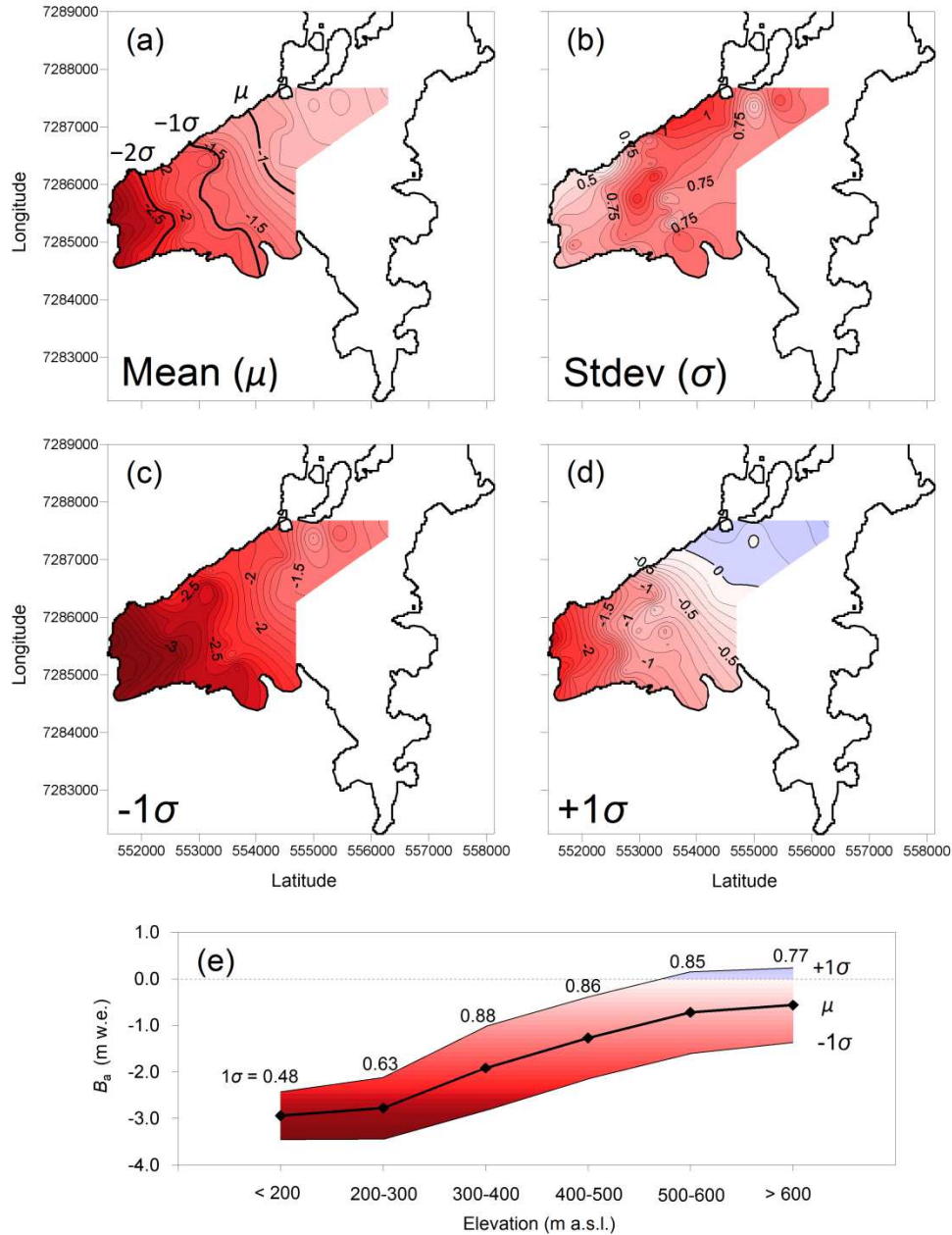
748

749



750
 751 **Figure 5:** Observed B_a , cumulative B_a , and linear trend for B_a for Mittivakkat Gletscher
 752 (1995/96–2013/14). The colors light blue and pink indicated B_a values one standard deviation
 753 above or below mean, respectively, and red color two standard deviations below mean B_a . For
 754 each B_a the errors from measurements and analytics are added.

755
 756
 757
 758
 759
 760
 761
 762
 763
 764
 765



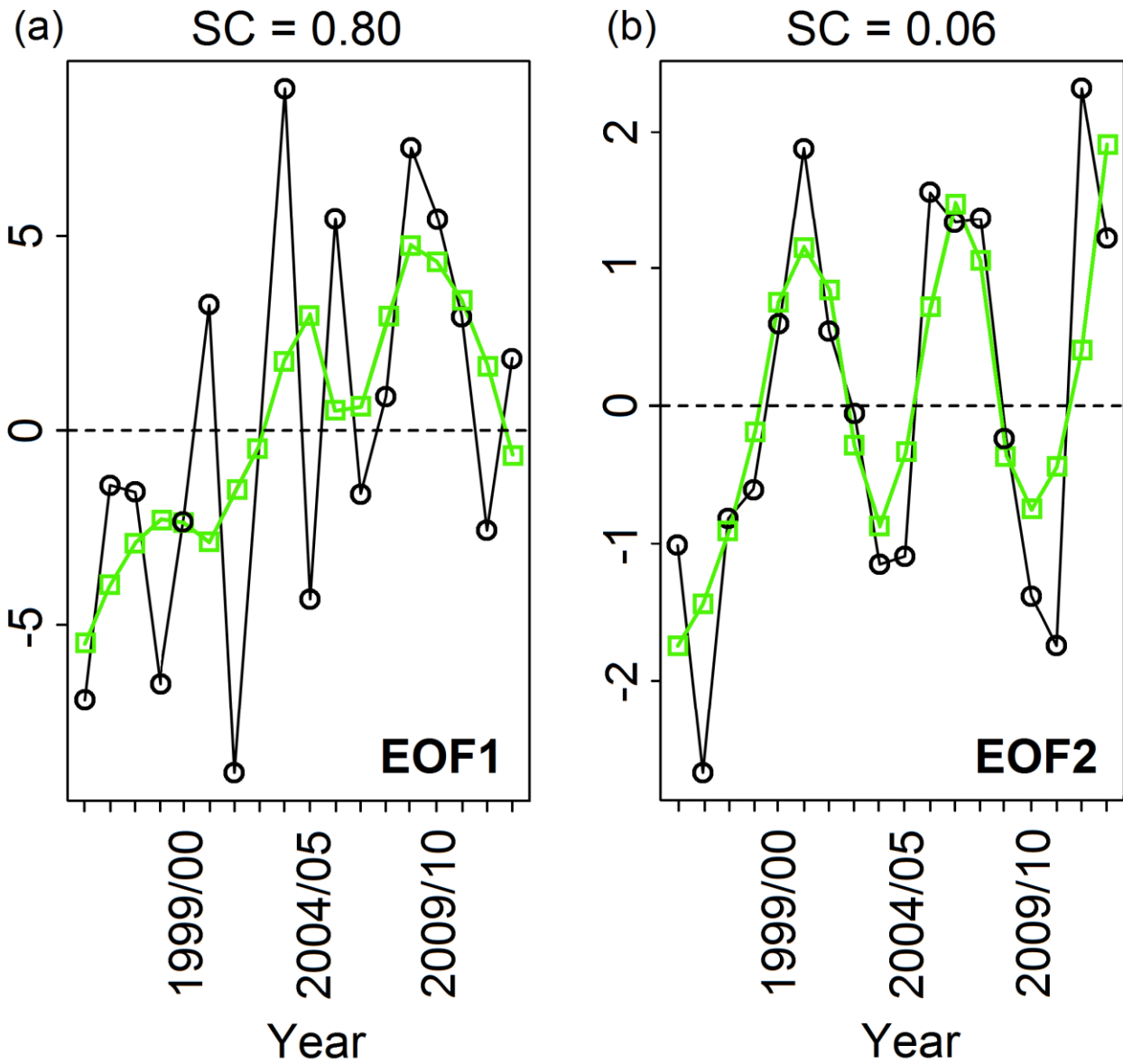
766

767 **Figure 6:** Observed Mittivakkat Gletscher (1996/97–2013/14): (a) spatial mean b_a (μ) where one
 768 (-1σ) and two (-2σ) standard deviations are illustrated with bold lines; (b) spatial distribution of
 769 one standard deviation (σ); (c) spatial b_a minus one standard deviation (-1σ); (d) spatial b_a plus
 770 one standard deviation ($+1\sigma$); and (e) longitudinal b_a profile with plus and minus one standard
 771 deviation.

772

773

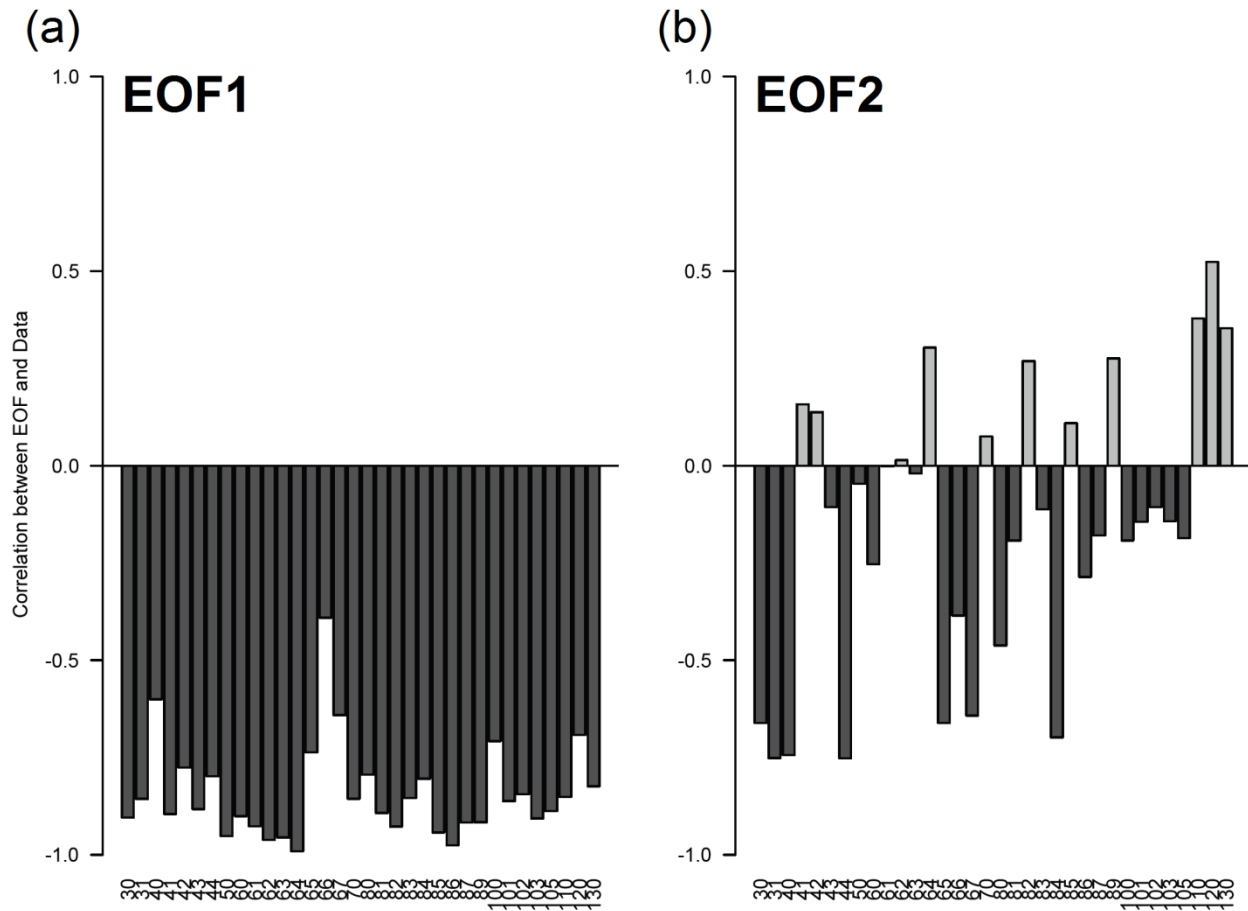
774



775

776 **Figure 7:** Mass-balance time series (1996/97–2013/14) based on the empirical orthogonal
 777 functions: (a) EOF1; and (b) EOF2. The explained square covariance (SC) is shown for each
 778 EOF. The green line is a five running mean smoothing line.

779



780

781 **Figure 8:** Eigenvector correlation values for each individual site for: (a) EOF1, and (b) EOF2.

782 Locations from left to right go from stake 30 to stake 130.

783

784

785

786

787

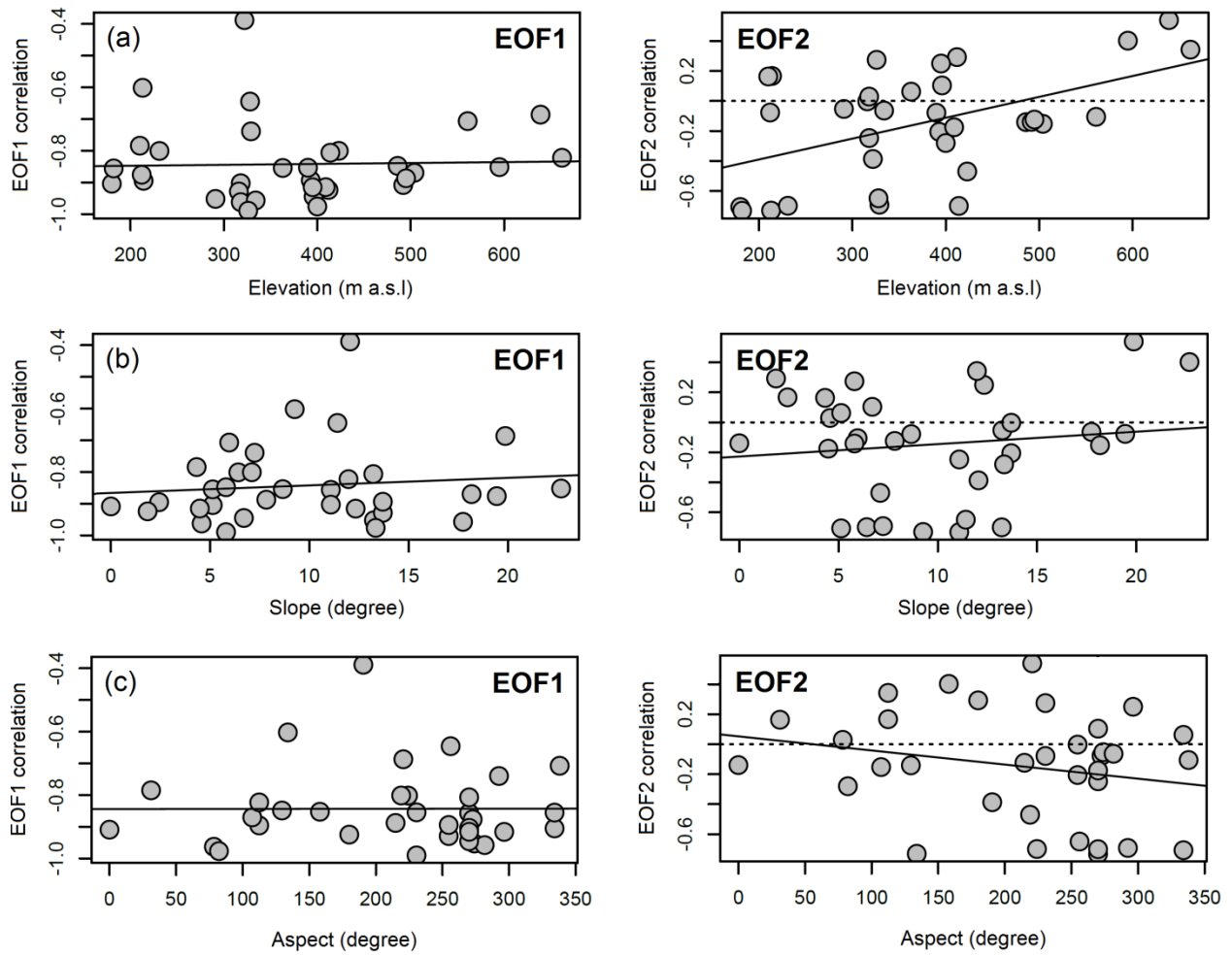
788

789

790

791

792



793

794 **Figure 9:** EOF1 and EOF2 correlations between: (a) stake elevation; (b) stake surface slope; and

795 (c) stake surface aspect.

796

797

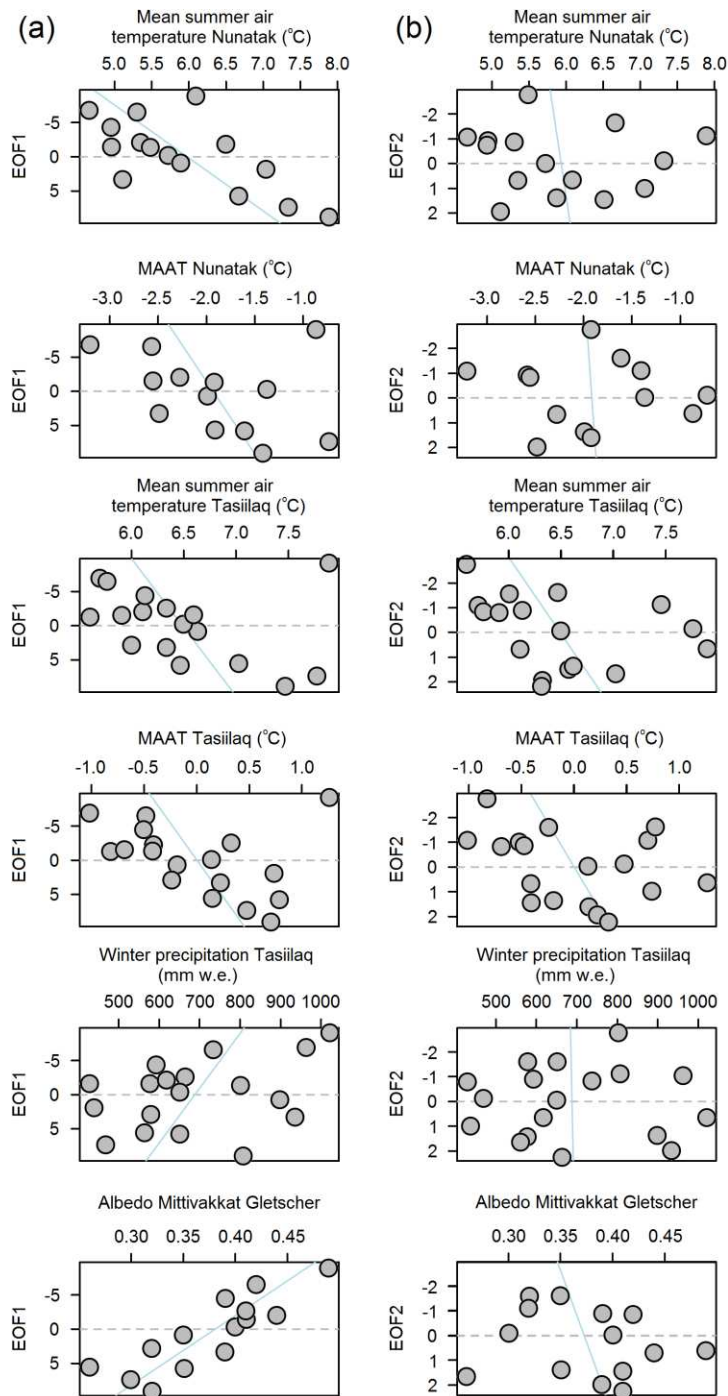
798

799

800

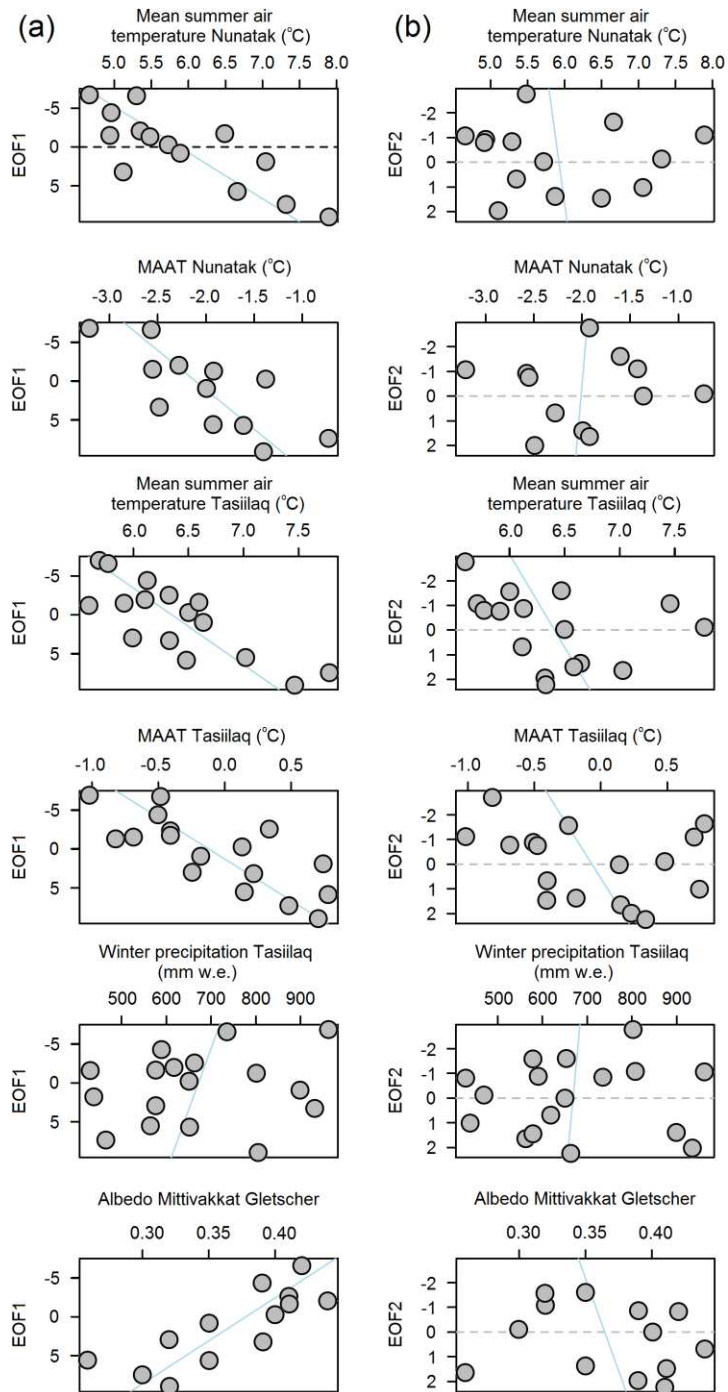
801

802



803

804 **Figure 10:** (a) EOF1; and (b) EOF2 correlations between Station Nunatak mean summer air
 805 temperature, Station Nunatak MAAT, Station Tasiilaq mean summer air temperature, Station
 806 Tasiilaq MAAT, Station Tasiilaq winter precipitation, and Mittivakkat Gletscher mean glacier-
 807 wide surface albedo by end of the mass-balance year for the 16-days mean period 27/28 July–
 808 12/13 August (Mernild et al. 2015b).



809

810 **Figure 11:** (a) EOF1; and EOF2 correlations without the statistical outlier from 2002 between
 811 Station Nunatak mean summer air temperature, Station Nunatak MAAT, Station Tasiilaq mean
 812 summer air temperature, Station Tasiilaq MAAT, Station Tasiilaq winter precipitation, and
 813 Mittivakkat Gletscher mean glacier-wide surface albedo by the end of the mass-balance year for
 814 the 16-days mean period 27/18 July–12/13 August (Mernild et al. 2015b).

815 **Table 1:** Mittivakkat Gletscher surface slope and aspect estimated from ASTER GDEM v2.

816

Slope (degrees)	Percentage of area and area	Aspect	Percentage of area and area
0–5	8.3 % (2.2 km ²)	North	11.5 % (3.0 km ²)
6–10	18.7 % (4.9 km ²)	Northeast	9.8 % (2.6 km ²)
11–15	20.0 % (5.2 km ²)	East	11.3 % (3.0 km ²)
16–20	18.2 % (4.8 km ²)	Southeast	8.8 % (2.2 km ²)
21–25	12.0 % (3.1 km ²)	South	11.2 % (2.9 km ²)
26–30	8.6 % (2.3 km ²)	Southwest	13.3 % (3.5 km ²)
31–35	5.6 % (1.4 km ²)	West	19.7 % (5.2 km ²)
36–40	3.6 % (0.9 km ²)		
41–45	2.2 % (0.6 km ²)	Northwest	14.4 % (3.8 km ²)
>45	2.9 % (0.8 km ²)		

817

818

819

820

821

822

823

824

825

826

827

828

829

830

831

832

833

834

835

836

837 **Table 2:** Statistical relationships between EOF1 and EOF2 and meteorological variables
838 observed near MG and MG mean glacier-wide surface albedo. The lower part of the table is
839 without the statistical outlier from 2002. The letter S = significant, and InS = insignificant.

All data					
Relationship		Slope	F-value	P-value	$p \leq 0.05$
EOF1	Mean summer air temperature (Station Nunatak)	5.98	12.37	0.00	S
	MAAT (Station Nunatak)	-1.93	1.81	0.21	InS
	Mean summer air temperature (Station Tasiilaq)	6.49	2.38	0.14	InS
	MAAT (Station Tasiilaq)	0.00	2.56	0.13	InS
	Winter precipitation sum (Station Tasiilaq)	688.22	2.19	0.16	InS
	Mean glacier-wide surface albedo	0.38	32.28	0.00	S
EOF2	Mean summer air temperature (Station Nunatak)	5.93	0.06	0.81	InS
	MAAT (Station Nunatak)	-1.92	1.94	0.18	InS
	Mean summer air temperature (Station Tasiilaq)	6.49	1.94	0.18	InS
	MAAT (Station Tasiilaq)	0.00	1.79	0.20	InS
	Winter precipitation sum (Station Tasiilaq)	688.22	0.00	0.97	InS
	Mean glacier-wide surface albedo	0.37	0.44	0.52	InS
All data except the statistical outlier from 2002					
EOF1	Mean summer air temperature (Station Nunatak)	5.88	23.11	0.00	S
	MAAT (Station Nunatak)	-2.11	13.74	0.00	S
	Mean summer air temperature (Station Tasiilaq)	6.35	23.59	0.00	S
	MAAT (Station Tasiilaq)	-0.12	21.63	0.00	S
	Winter precipitation sum (Station Tasiilaq)	672.09	0.49	0.50	InS
	Mean glacier-wide surface albedo	0.38	19.21	0.00	S
EOF2	Mean summer air temperature (Station Nunatak)	5.92	0.05	0.84	InS
	MAAT (Station Nunatak)	-2.01	1.64	0.22	InS
	Mean summer air temperature (Station Tasiilaq)	6.41	1.64	0.22	InS
	MAAT (Station Tasiilaq)	-0.07	1.53	0.24	InS
	Winter precipitation sum (Station Tasiilaq)	668.51	0.03	0.86	InS
	Mean glacier-wide surface albedo	0.37	0.33	0.58	InS

840